Surface-Enhanced Raman Scattering on Aggregates of Platinum Nanoparticles with Definite Size

Kwan Kim,[†,*] Kyung Lock Kim,[†] Hyang Bong Lee,[†] and Kuan Soo Shin[‡,*]

Department of Chemistry, Seoul National University, Seoul 151-742, Korea and Department of Chemistry, Soongsil University, Seoul 156-743, Korea

Received: August 19, 2010; Revised Manuscript Received: September 27, 2010

Platinum nanoparticles with nominal diameters of 28 to 105 nm were prepared by a multistep seed-mediated growth method and the surface-enhanced Raman scattering (SERS) characteristics of their aggregates were examined. In the film state, a broad but distinct UV−vis absorption band occurred at ∼330 nm, regardless of the size of the Pt particles, but with higher absorbance from a film assembled with larger Pt particles. Higher Raman intensity was thus observed at shorter excitation wavelengths from adsorbates on a Pt film made of 105 nm sized Pt particles, in agreement with the electromagnetic enhancement mechanism. The enhancement factor (EF), determined to be 1.5×10^2 at 514.5 nm excitation, was, however, an order of magnitude smaller than that of our earlier Pt film fabricated with laser-ablated 17 nm sized particles. Consulting the X-ray diffraction analyses, the smaller EF value was attributed to the fact that all Pt particles prepared in this work via a seed-mediated growth method were actually composed of 7.2 nm sized seed particles. Even with lower EF values, we were able to successfully characterize the SERS characteristics of two typical aromatic thiols, 4-nirobenzenethiol (4-NBT) and 4-aminobenzenethiol (4-ABT). Specifically, we found that 4-NBT is barely subjected to photoreaction on a Pt surface, in contrast with that on Ag. We found also that the chemical enhancement mechanism is operating, along with the electromagnetic enhancement mechanism, in the SERS of 4-ABT on Pt to show its b_2-type bands, similarly to that on Ag.

1. Introduction

Since the discovery of surface-enhanced Raman scattering (SERS) in the 1970s, there have been extensive theoretical and experimental studies of this effect.[1−16] In recent years, it has been reported that even single-molecule spectroscopy is possible by SERS, suggesting that the enhancement factor (EF) can reach as much as $10^{14}-10^{15}$.[6−11] One can therefore readily acquire vibrational spectra from adsorbates on roughened noble metals such as silver and gold. How about other metals? Regarding SERS, two enhancement mechanisms − one called the long-range electromagnetic (EM) effect and the other called the short-range chemical or charge-transfer effect − are believed to be simultaneously operational at metal−adsorbate interfaces.[3−12] A challenging issue in nanoscience is the fabrication of nanostructures that exhibit a large EM effect.[12−16] In line with this, Tian and his colleagues reported that even transition metals could be made to be SERS-active, via an electrochemical roughening process, with the EFs ranging from 1 to 3 orders of magnitude.[17−22] On the other hand, an attenuated total reflection (ATR) method to excite the surface plasmon polariton (SPP) was applied to transition metals like platinum, as well as noble metals to improve the sensitivity level of classical Raman spectroscopy.[23,24] However, it is still difficult to obtain Raman spectra of molecules adsorbed on transition metals like platinum, especially in nonelectrochemical environments or without a sophisticated ATR-SPP setup.

For SERS to occur via the EM enhancement mechanism, the Raman excitation wavelength has to be close to that of the surface plasmon oscillation of metal nanoparticles or nanoaggregates. Earlier, Creighton and Eadon calculated the optical absorption of platinum nanoparticles based on the Mie theory and showed that a plasmon peak should appear at 215 nm.[25] Experimentally, Henglein et al. showed that a peak really exists around 215 nm for nanoparticles prepared by the radiolytic reduction of $PtCl_4^{2-}$.[26,27] So far, the platinum particles prepared by the chemical reduction of $PtCl_4^{2-}$ are mostly smaller than ∼10 nm, showing negligible absorption in the visible region. This suggests that SERS spectra are hard to obtain for molecules assembled on platinum nanoparticles, at least under visible light excitation and in a nonelectrochemical environment.

Some years ago, we were able to record SERS spectra, even with visible excitation, for organic monolayers assembled on Pt nanoparticles, specifically those with diameters of ∼17 nm, prepared by a laser-ablation method.[28−30] In that work, the EF estimated using benzenethiol as a model adsorbate was as large as 1.4×10^3 with an excitation of 514.5 nm.[28] In the UV−vis spectra, no characteristic peak was identified in the sol state but a very broad band developed around 550 nm as 17 nm sized Pt particles were deposited onto an indium tin oxide (ITO) substrate. Accordingly, the origin of the Raman enhancement at Pt nanoaggregates was assumed to be electromagnetic. Since then, it has been questioned whether the EM effect would increase further using Pt particles greater than 17 nm.

Very recently, it has been reported by Bigall et al. that Pt particles even greater than 100 nm can be prepared in laboratory conditions.[31] The SERS characteristics of those Pt nanoparticles films have thus been investigated in this work. Specifically, Pt particles with a nominal diameter of 28, 46, 72, and 105 nm were prepared and then the particles were packed into columns

* To whom correspondence should be addressed. E-mail: kwankim@snu.ac.kr. Tel: +82-2-8806651. Fax: +82-2-8891568 (K.K.), E-mail: kshin@ssu.ac.kr. Tel: +82-2-8200436. Fax: +82-2-8244383 (K.S.S.).
† Seoul National University.
‡ Soongsil University.

10.1021/jp1078532
Published on Web 10/12/2010

(film appearance). In that way, a higher extinction in the visible region was observed from the film assembled with larger Pt particles. The highest EF was obtained from a film comprised of 105 nm sized Pt particles, in agreement with the EM enhancement mechanism. The EF of the film was not, however, greater than that of our earlier film fabricated using laser-ablated 17 nm sized Pt nanoparticles. This unexpected observation was explained by the fact that the Pt nanoparticles prepared by a seed-mediated growth method were actually composed of smaller (~7 nm in diameter) particles.

2. Experimental Section

Chloroplatinic acid hexahydrate ($H_2PtCl_6 \cdot 6H_2O$), sodium citrate, sodium borohydride, L-ascorbic acid, 3-aminopropyltrimethoxysilane (3-APS), benzenethiol (BT), 4-aminobenzenethiol (4-ABT), and 4-nitrobenzenethiol (4-NBT) were purchased from Aldrich and used as received. Other chemicals unless specified were reagent grade, and triply distilled water of resistivity greater than 18.0 MΩ·cm (Millipore Milli-Q System) was used in preparing aqueous solutions.

Platinum sols were prepared by following the seed-mediated growth method reported by Bigall et al.[31] Initially, small platinum seeds of 5−7 nm diameter were prepared. At first, 3 mL of a 0.2% solution of chloroplatinic acid hexahydrate was added to 39 mL of boiling deionized water. After 1 min, 0.92 mL of 1% sodium citrate was added, followed half a minute later by a quick injection of 0.46 mL of a freshly prepared 0.08% solution of sodium borohydride also containing 1% sodium citrate. After 10 min, the sol solution was cooled down to room temperature. The seeds obtained in this way were used in preparing ~30 nm sized Pt particles. Specifically, to 30 mL of deionized water was added consecutively 1 mL of the platinum seed solution, 0.045 mL of 0.4 M chloroplatinic acid solution, and then 0.5 mL of 1.25% L-ascorbic acid solution containing also 1% sodium citrate. The mixture was slowly heated to the boiling point and left to boil for 30 min with stirring. According to the transmission electron microscopy (TEM) analysis, the size of the Pt nanoparticles was 28 nm (vide infra). These 28 nm sized Pt particles were used as seeds in preparing ~46 nm sized Pt particles. The reaction mixture for 46 nm sized Pt particles was comprised of 26 mL of deionized water, 1 mL of 28 nm sized Pt solution, 0.045 mL of chloroplatinic acid, and a 0.5 mL mixture solution of 1% sodium citrate and 1.25% L-ascorbic acid. To prepare 72 (or 105) nm sized Pt particles, the reaction mixture was comprised of 29 mL of deionized water, 1 (or 0.25) mL of 46 (or 72) nm sized Pt solution, 0.045 mL of chloroplatinic acid, and a 0.5 mL mixture solution of 1% sodium citrate, and 1.25% L-ascorbic acid. As before, the reaction mixture was boiled for 30 min with stirring, and then cooled down to room temperature. The reaction products gathered by centrifugation (Centrifuge operated at 1000−13500 rpm depending on the nanoparticle size) were washed three times with deionized water, and then stored by dispersing in water.

Pt nanoaggregate films were prepared by dropping the above Pt sol solution onto an ITO or Si wafer. Initially, the ITO and Si wafers were subjected to ozonolysis to render them hydrophilic at a water contact angle <5°. They were subsequently reacted with 3-APS, following the protocol given in the literature,[32] in order to possess amine-terminated functionalities. A Viton O-ring of i.d. 5 mm was subsequently placed on the ITO or Si wafer, and then multiples of 10 μL of Pt sol were injected inside the O-ring. The injected substrate was left to dry under ambient conditions to form a uniform and circular nanoaggregate film. The film was washed with deionized water and then dried under an N_2 atmosphere. Six different Pt nanoaggregate films were prepared by injecting 10, 20, 30, 40, 50, and 60 μL of Pt sol onto an ITO or Si wafer, and their dried films were named S1, S2, S3, S4, S5 and S6, respectively. These Pt films were cleaned in an electrochemical cell via a hydrogen evolution reaction. When adsorbing organic probe molecules onto Pt, the Pt nanoaggregate films were soaked in 5 mM ethanolic solution of BT or 4-ABT for 1 h and then washed with ethanol.

TEM images of Pt nanoparticles were acquired using a JEM-200CX transmission electron microscope at 160 kV. The X-ray diffraction (XRD) and field emission scanning electron microscope (FE-SEM) image of Pt aggregates on a silicon wafer were obtained with a Philips X'PERT-MPD diffractometer for a 2θ range of 5−80° at an angular resolution of 0.02° using Cu Kα (1.5419 Å) radiation and a JSM-6700F FE-SEM operated at 5.0 kV, respectively. UV−vis extinction spectra were obtained with a SINCO S-4100 UV−vis absorption spectrometer. Cyclic voltamograms (CVs) of Pt aggregates on ITO were recorded in 0.5 M aqueous H_2SO_4 using a CH Instrument Model 600A potentiostat, which employed CHI 600A Electrochemical Analyzer software (version 2.03) running on an IBM-compatible PC. The reference electrode was a saturated calomel electrode (SCE), and a platinum spiral wire was used as the counter electrode. Before initiating any CV measurement, the electrolyte solution was deaerated with high-purity N_2 gas.

Raman spectra were obtained using a Renishaw Raman system Model 2000 spectrometer equipped with an integral microscope (Olympus BH2-UMA). The 514.5 nm line from a 20 mW Ar^+ laser (Melles-Griot Model 351MA520) or the 488 and 568 nm lines from a 20 mW Ar^+/Kr^+ laser (Melles-Griot Model 35KAP431) or the 632.8 nm line from a 17 mW He/Ne laser (Spectra Physics Model 127) were used as the excitation source. Raman scattering was detected over a 180° range with a Peltier cooled (−70 °C) charged-coupled device (CCD) camera (400 × 600 pixels). The laser beam was focused onto a spot approximately 1 μm in diameter with an objective microscope with a magnification of the order of 20×. The data acquisition time was usually 60 s. The Raman band of a silicon wafer at 520 cm^{-1} was used to calibrate the spectrometer.

3. Results and Discussion

Part a of Figure 1 shows the TEM images of four different Pt nanoparticles prepared in this work. Note that they are mostly spherical and, according to the histograms in part b of Figure 1, their mean diameters are determined to be either 28 ± 7 or 46 ± 5 or 72 ± 4 or 105 ± 6 nm: the particles are highly monodispersed at all sizes. Part c of Figure 1 shows the UV−vis extinction spectra of these Pt particles in a colloidal state: the particle concentrations are the same in all UV−vis spectra. As can be seen in part d of Figure 1, the wavelength of the peak maximum associated with the surface plasmon resonance is red-shifted from 250 to 500 nm almost linearly in proportion to the size of Pt nanoparticles.

Part a of Figure 2 shows the UV−vis spectra of Pt nanoparticles films assembled on ITO. Hereafter, the film made of 60 μL of 28 nm sized Pt sol on ITO, for instance, is labeled S6(Pt-28 nm)/ITO, and others are similarly labeled: remember that particle concentration was the same in all Pt sols. For all Pt films, a broad but distinct band occurs at ~330 nm, and then the absorbance decreases slowly until reaching a minimum in the infrared region: the absorbance itself is increasing with an increase in the size of the Pt nanoparticles. Different spectral

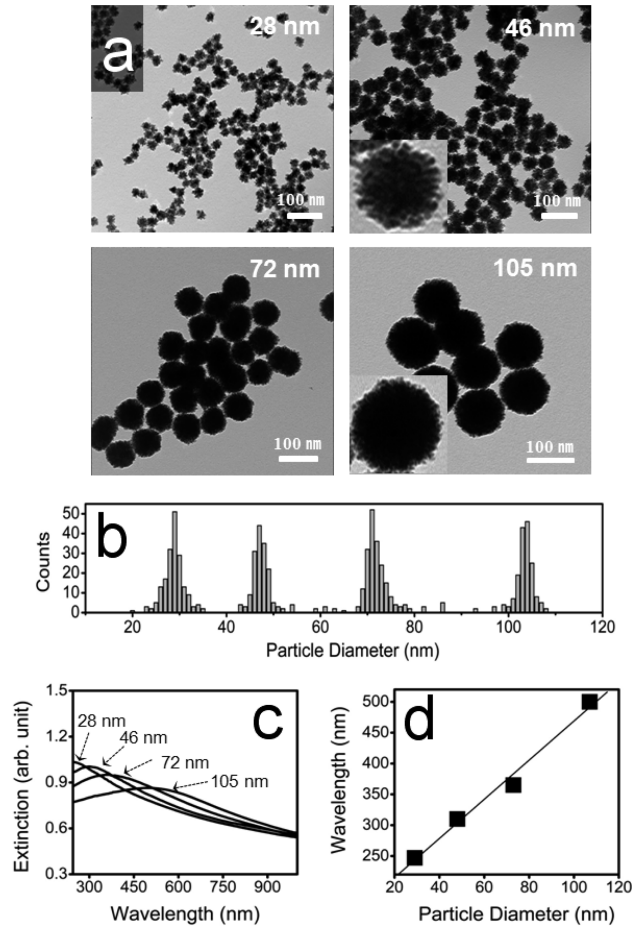

Figure 1. (a) TEM images of four different Pt nanoparticles and (b) their histograms; the magnified TEM images of 46 nm sized and 105 nm sized Pt nanoparticles are also shown in the insets. (c) UV−vis extinction spectra of Pt nanoparticles in a colloidal state (particle concentrations are the same in all spectra) and (d) the peak maximum drawn versus the size of Pt nanoparticles.

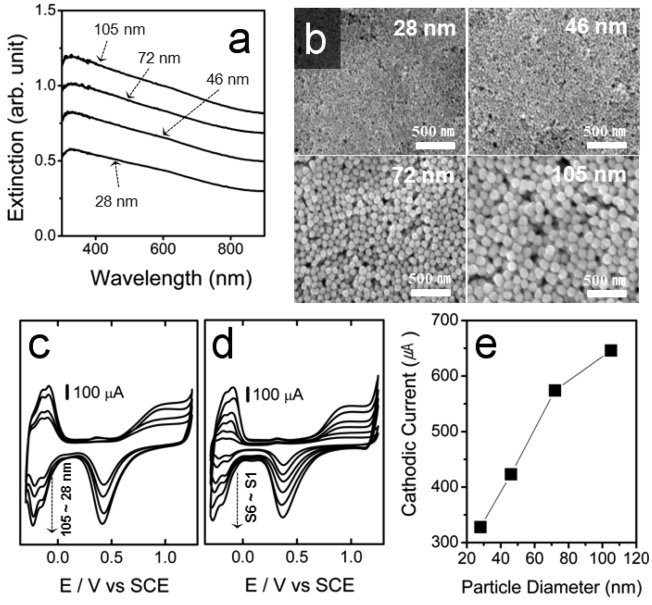

Figure 2. (a) UV−vis spectra of Pt S6 films assembled on ITO: See text. (b) FE-SEM images of Pt S6 films assembled on silicon wafers. (c) CVs of Pt S6 films in 0.1 M H_2SO_4 solution (scan rate = 0.05 V/s) (d) CVs of Pt S1∼S6 films fabricated using 105 nm sized Pt particles. (e) Cathodic current in (c) drawn versus size of Pt particles used in fabricating S6 films.

changes compared with the colloid samples must be attributable to the close-packed structure of Pt nanoparticles in the film state. Part b of Figure 2 shows the FE-SEM images of four S6 films with different particle diameters assembled on silicon wafers, that is, S6(Pt-28 nm)/ITO, S6(Pt-46 nm)/ITO, S6(Pt-72 nm)/ITO, and S6(Pt-105 nm)/ITO. In all films, the Pt particles are packed closely as expected.

Part c of Figure 2 shows the CVs of the four S6 films, comprised of differently sized Pt nanoparticles, measured by potential cycling between −0.30 and +1.25 at 0.05 V/s in an aqueous 0.1 M H_2SO_4 solution. All CV profiles are identical and also similar to that obtained with a conventional polycrystalline Pt electrode under the same conditions.[33−38] The peak appearing at −0.22 V at the cathodic site is due to the reduction of protons to gaseous hydrogen, and the peak around 0.4 V is associated with the desorption of gaseous oxygen. As expected, the cathodic current increases in proportion to the number of layers of Pt particles. Part d of Figure 2 shows the CVs measured using S1−S6 electrodes fabricated with 105 nm sized Pt particles. As can be seen in part e of Figure 2, the redox current also increases proportionally to the size of Pt particles in S6 films: A larger cathodic current is measured when larger particles are packed together. Recalling the fact that the charge density associated with the adsorption and desorption of H atoms on a polycrystalline Pt electrode amounts to 210 $\mu C/cm^2$,[33] the roughness factors of the S6(Pt-28 nm)/ITO, S6(Pt-46 nm)/ITO, S6(Pt-72 nm)/ITO, and S6(Pt-105 nm)/ITO films are determined to be 109, 137, 182, and 213, respectively. Similarly, the roughness factors of the S1 to S5 films assembled from 105 nm Pt particles are 25, 61, 89, 128, and 157, respectively. Hence, the S6(Pt-105 nm)/ITO film has, among others, the highest electrochemical roughness factor in this work.

Part a of Figure 3 shows the Raman spectra of BT adsorbed on four different S6 films measured using 514.5 nm radiation as the excitation source. The strongest Raman signal was observed from the S6(Pt-105 nm)/ITO film. All the peaks can be attributed to BT.[39,40] This is evident by comparing it with the normal Raman (NR) spectrum of BT, also shown in part a of Figure 3. In the NR spectrum, the peaks at 3058, 1571, and 999 cm^{-1} are due to CH stretching, ring CC stretching (ν_{8a}), and ring CCC in-plane bending (ν_{12}) modes of BT respectively, whereas the peaks at 2567 and 917 cm^{-1} are due to SH stretching and CSH bending vibration, respectively. In the Raman spectra of BT on Pt, one cannot find the counterparts of the latter two vibrational bands. Otherwise, all the peaks can be correlated with those in the NR spectrum. The absence of the SH group bands can be understood by presuming that BT is adsorbed on Pt as a thiolate by forming a Pt−S bond.[39,40]

In part b of Figure 3 is collectively summarized the variation in peak intensity of the ν_{8a} band of BT (normalized with respect to that of silicon wafer at 520 cm^{-1}) measured at 514.5 nm excitation in terms of the number of layers of four different Pt particles. Overall, a stronger signal is observed in the order of S6 > S5 > S4 > S3 > S2 > S1 films. However, for the films assembled with 72 and 105 nm sized Pt particles, the Raman signal becomes saturated by the signal from the S4 films. Maxwell et al. reported a similar leveling off behavior of SERS intensity from a nanostructured thin film made of Ag nanoparticles.[41]

In part c of Figure 3 is collectively summarized the variation in peak intensity of the ν_{8a} band of BT on S6 films in terms of the size of Pt nanoparticles and the excitation wavelengths. Signal strength is observed in the order of size of the Pt particles, that is 105 > 72 > 46 > 28 nm, and 488 > 514.5 > 568 > 632.8

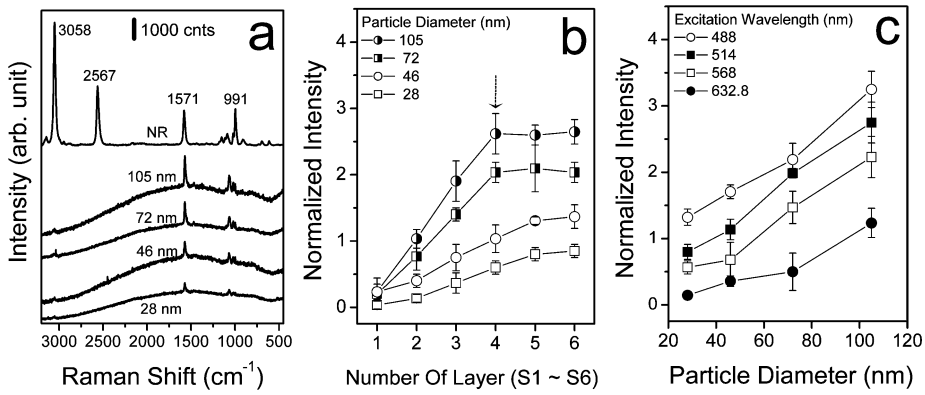

Figure 3. (a) Raman spectra of BT adsorbed on four different Pt S6 films, i.e., S6(Pt-28 nm)/ITO, S6(Pt-46 nm)/ITO, S6(Pt-72 nm)/ITO, and S6(Pt-105 nm)/ITO films, measured at 514.5 nm excitation: For comparison, the NR spectrum of BT in the neat state is also shown. (b) Peak intensity of ν_{8a} band of BT (normalized with respect to that of a silicon wafer at 520 cm^{-1}) measured at 514.5 nm excitation drawn versus the number of layers (S1∼S6) of four different Pt particles. (c) Normalized peak intensity of the ν_{8a} band of BT on S6 films drawn versus the size of Pt nanoparticles, as well as the excitation wavelengths.

nm excitation. This correlates with the variation of the UV−vis absorbance of Pt films shown in part a of Figure 2, suggesting that the electromagnetic enhancement mechanism is indeed operative in these films to show a strong SERS signal. On the other hand, the fact that the Raman signal is strongly dependent on the size of the Pt particles suggests that the chemical enhancement mechanism is rather insignificant in the present system. As observed here, the S4∼S6(Pt-105 nm)/ITO films exhibited the strongest Raman signal for BT, so that subsequent measurements were conducted using those kind of films. In particular, the surface enhancement factor (EF) was estimated using the S4(Pt-105 nm)/ITO film.

To estimate the EF,[42] we use the following relationship: EF $= (I_{SERS}/I_{NR})(N_{NR}/N_{SERS})$ in which I_{SERS} and I_{NR} are the SERS intensity of BT on Pt and the NR intensity of BT in bulk, respectively, and N_{SERS} and N_{NR} are the number of BT molecules illuminated by the laser light to obtain the corresponding SERS and NR spectra, respectively. I_{SERS} and I_{NR} were measured for the ν_{8a} band and N_{SERS} and N_{NR} were calculated on the basis of the estimated concentration of surface BT species, the density of bulk BT, and the sampling areas. The surface concentration of BT on S4(Pt-105 nm)/ITO is assumed to be the same as that on gold and silver, that is $\sim 7.1 \times 10^{-10}$ mol/cm^2.[43] Taking the sampling area (ca. 1 μm in diameter) as well as the surface roughness factor (∼128) into account, $N_{SERS} = 7.1 \times 10^{-16}$ mol. When taking the NR spectrum of pure BT, the sampling volume will be the product of the laser spot and the penetration depth (∼15 μm) of the focused beam; in a separate experiment, we confirmed that the Raman signal reaches a steady state when the thickness of an organic film becomes greater than 15 μm. As the density of BT is 1.07 g/cm^3, N_{NR} is calculated to be 1.1×10^{-13} mol. Because the intensity ratio, I_{SERS}/I_{NR}, is measured to be ∼1 at 514.5 nm excitation, EF can then be as large as 1.5×10^2. This clearly indicates that SERS can be induced to occur even on a Pt substrate by visible laser irradiation. Nonetheless, it is also disappointing that the EF of a Pt film comprised of 105 nm sized particles is smaller than that ($\sim 1.4 \times 10^3$) of our earlier Pt film fabricated with laser-ablated 17 nm sized particles: Here, the earlier reported value, 1.9×10^2, is modified to 1.4×10^3 by considering the newly estimated penetration depth of the laser beam.

A clue to explain the lower EF values is obtained from the XRD data. Parts a and b of Figure 4 show the XRDs of two S6 Pt films fabricated with either the initial seed particles or the 105 nm sized particles. For comparison, the XRD of a Pt film

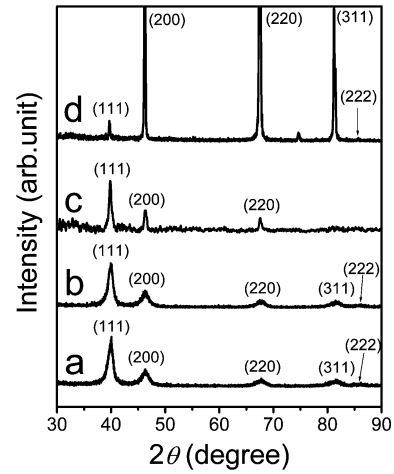

Figure 4. XRDs of (a) S6(Pt-7 nm) and (b) S6(Pt-105 nm) films assembled on silicon wafers: For comparison, the XRDs of (c) Pt laser-ablated sol film and (d) a polycrystalline Pt foil are also shown.

comprised of laser-ablated particles, as well as that of a polycrystalline Pt foil, were also included in parts c and d of Figure 4. In all diffractograms, the peaks at 2θ values of 39.7°, 46.2°, 67.4°, and 81.2° can be attributed to the reflections of (111), (200), (220), and (311) crystalline planes of cubic Pt, respectively. It is seen that the (111) peak is dominant in the XRD of Pt particle films, although the peak is negligibly weak in the XRD of a Pt foil: the intensity ratio of the (111) and (200) reflections, that is $I_{(111)}/I_{(200)}$, is 2.9 (Pt seed), 2.9 (Pt 105 nm), 2.4 (Pt laser), and 0.07 (Pt foil). This suggests that the (111) surface is energetically the most favorable in the nanoparticle realm: Pt nanoparticles prepared by chemical method in this work exhibit the (111) surface more abundantly than those prepared by laser ablation method. Another noteworthy point in Figure 4 is that there are significant differences in the bandwidths. Using the Scherrer equation,[44] we have estimated the average sizes of Pt particles by analyzing the (111) peak widths at half-maximum of the XRD data. The sizes determined were 7.1 nm (Pt seed), 7.2 nm (Pt 105 nm), 16 nm (Pt laser), and 57 nm (Pt foil). We already reported that the size of laser ablated Pt particles determined by TEM analysis (17 nm) is hardly different from that determined by the analysis of XRD peaks (16 nm).[28] For the film assembled in this work using Pt seeds, the TEM and XRD analyses also resulted in the same size (∼7 nm). However, the film supposedly composed of 105 nm sized Pt particles (in accordance with the TEM analysis)

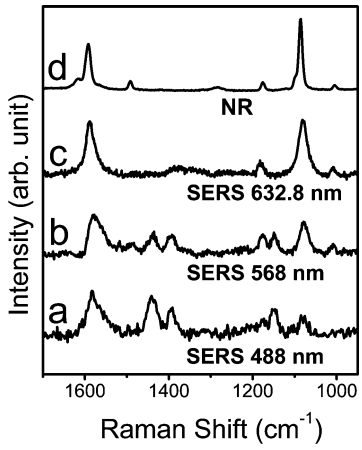

Figure 5. SERS spectra of 4-ABT on S6(Pt-105 nm)/ITO film taken using (a) 488, (b) 568, and (c) 632.8 nm radiation as the excitation source: (d) NR spectrum of 4-ABT in neat solid state taken at 568 nm excitation.

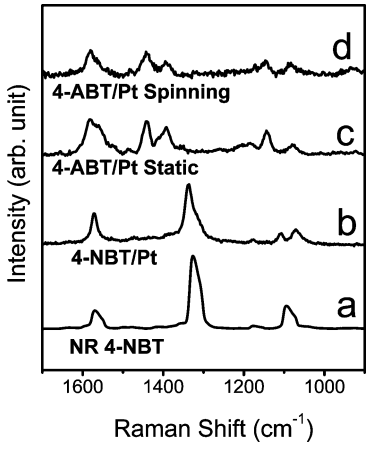

Figure 6. (a) NR spectrum of 4-NBT in neat solid state and (b) SERS spectrum of 4-NBT on S6(Pt-105 nm)/ITO film measured at 488 nm excitation. SERS spectra of 4-ABT on S6(Pt-105 nm)/ITO measured under (c) static and (d) spinning at 3000 rpm at 488 nm excitation.

turns out, from the XRD analysis, to be comprised of 7.2 nm sized particles. The latter size is exactly the same as that of the seed. Hence, all Pt nanoparticles prepared here by a seed-mediated growth method are assumed to consist of smaller (~7 nm in diameter) particles; magnified TEM images of the 46 nm sized and 105 nm sized Pt nanoparticles composed of ~7 nanometer sized particles are shown in the inserts of part a of Figure 1. This must be why the EF of a Pt film comprised of 105 nm sized particles was smaller than that of a Pt film fabricated using laser-ablated particles.[45]

Parts a, b, and c of Figure 5 show the Raman spectra of 4-ABT on a S6(Pt-105 nm)/ITO film taken using 488, 568, and 632.8 nm radiation as the excitation source, respectively. For comparison, the NR spectrum of 4-ABT is shown in part d of Figure 5. The NR spectral pattern of 4-ABT is independent of the excitation wavelength but it is seen in parts a, b, and c of Figure 5 that the SERS spectral pattern of 4-ABT on Pt is highly dependent on the excitation wavelength. All of the SERS peaks of 4-ABT in part c of Figure 5 can be correlated with those in the NR spectrum in part d of Figure 5. In the SERS spectra in parts a and b of Figure 5, however, there are additional peaks present that are difficult to correlate with the NR peaks in part d of Figure 5. For a long time, those bands were classified as the b_2 type bands of 4-ABT and their appearance in the SERS spectra (on Ag nanoaggregates) was attributed to the involvement of the chemical enhancement mechanism in SERS.[46] Figure 5 clearly shows that the b_2 type bands, which are markers for chemical enhancement, are increasing in relative intensity toward shorter wavelength; this indicates an onset of a charge-transfer resonance in the SERS spectral feature of 4-ABT on Pt. Very recently, however, Tian et al. reported that those bands (observable using a roughened Ag electrode) should result from the photoreaction of 4-ABT, most probably azo molecules.[47] Nonetheless, the fact that such bands can be seen even in a nanogap electrode, in which 4-ABT is first self-assembled on planar Au and then Au (or Ag) nanoparticles are adsorbed on the pendent amine groups, suggests that the photoreaction may not be the sole reason for the appearance of those bands.[48−50] We have thus examined the Raman spectral feature of 4-ABT on Pt in more detail by measuring spectra not only at different excitation wavelengths but also at different potentials.

We examined, first, whether the Pt film is photoactive. It is well-known that 4-NBT on Ag is converted to give a SERS spectrum of 4-ABT by the irradiation of a visible laser.[51−55] As shown in part b of Figure 6, the SERS spectrum of 4-NBT assembled on a S6(Pt-105 nm)/ITO film is invariant, however, even after prolonged exposure to 488 nm radiation. For comparison, the NR spectrum of 4-NBT is also shown in part a of Figure 6. On the other hand, we have to mention that, as can be seen in parts c and d of Figure 6, the SERS spectral pattern of 4-ABT on Pt is also invariant, regardless of the spinning of the sample even up to 3000 rpm, as long as the excitation wavelength is fixed. These observations suggest that 4-ABT is hardly subjected to photoreaction on a Pt surface. The additional peaks observed in parts a and b of Figure 5 would then be due to the b_2-type bands of 4-ABT, not due to a

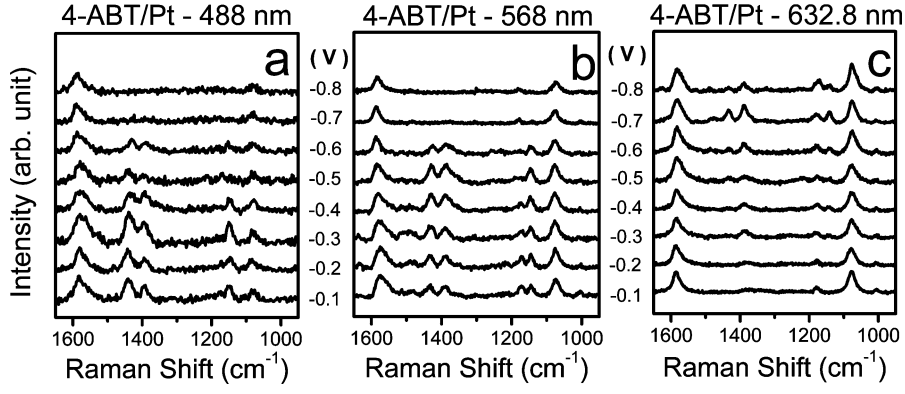

Figure 7. Potential-dependent SERS spectra of 4-ABT on S6(Pt-105 nm)/ITO measured using (a) 488, (b) 568, and (c) 632.8 nm radiation as the excitation source.

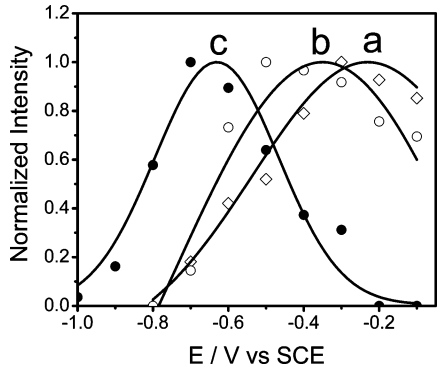

Figure 8. Normalized peak intensity of ring 19b band at 1439 cm^{-1} in Figure 7 drawn versus the electrode potential at (a) 488 or (b) 568 or (c) 632.8 nm excitation: Solid lines represent the Gaussian fitting.

photoreaction product like an azo compound. On this basis, we have measured the potential-dependent SERS spectra of 4-ABT on Pt at various excitation wavelengths.

Parts a, b, and c of Figure 7 show the potential-dependent SERS spectra of 4-ABT measured using 488, 568, and 632.8 nm radiation as the excitation sources, respectively. Note that all the spectra were reversibly observed during the potential cycling between −0.1 and −0.8 V. Variation in the SERS spectral pattern of 4-ABT on Pt is affected, however, not only by the electrode potential but also by the excitation wavelength. This is evident from Figure 8, which shows the normalized peak intensity of the ring 19b band, a typical b_2-type band of 4-ABT, drawn versus the electrode potential at three different excitation wavelengths. The solid lines in Figure 8 represent the Gaussian fitting of the peak intensities. At higher excitation wavelengths, the peak maximum (E_{max}) occurs at lower electrode potentials: at −0.63 V at 632.8 nm (1.96 eV) excitation, at −0.35 V at 568 nm (2.19 eV) excitation, and at −0.24 V at 488 nm (2.54 eV) excitation. The $dE_{max}/d(h\nu)$ slope, the slope of the peak maximum as a function of excitation energy, obtained in this work by the linear fitting is 0.993 V/eV. The positive slope of the curve and the fact that it is close to unity can be taken as the evidence of the metal to molecule charge-transfer nature of the spectral intensities.[56] This can be understood by presuming that the b_2-type bands are associated with a chemical enhancement mechanism in SERS, similar to that claimed by Osawa et al. for 4-ABT adsorbed on Ag electrodes.[46]

4. Summary and Conclusions

Four different Pt nanoparticles with nominal diameters of 28, 46, 72, and 105 nm were prepared by a seed-mediated growth method. Their UV−vis absorption maximum associated with the surface plasmon resonance varied almost linearly from 250 to 500 nm in proportion to the size of the Pt nanoparticles. When assembled into films on ITO, regardless of the size of the Pt nanoparticles, a broad but distinct band occurred at ∼330 nm, and then the absorbance decreased slowly until reaching a minimum in the infrared region: A higher absorbance was, however, observed from a film assembled with larger Pt particles. In agreement with the electromagnetic enhancement mechanism in SERS, a higher Raman intensity was observed at shorter excitation wavelengths from adsorbates on a Pt film made of 105 nm sized Pt particles. The enhancement factor (EF) determined at 514.5 nm excitation was, however, at best 1.5×10^2, which is about an order of magnitude smaller than that of our earlier Pt film fabricated with laser-ablated 17 nm sized particles. Consulting the XRD analyses, the smaller EF value was attributed to the fact that even the 105 nm sized Pt particles were, in fact, composed of 7.2 nm sized seed particles. Additionally, using the Pt film assembled in this work, we found that 4-NBT is only weakly photoreactive, in contrast with that on Ag. In addition, we found that the SERS spectral pattern of 4-ABT on Pt is variable not only with changes in the electrode potential but also by altering the excitation wavelength. These spectral variations could be understood by presuming that the chemical enhancement mechanism is also operating in this system, along with the electromagnetic enhancement, to show the b_2-type bands of 4-ABT similarly to that on Ag electrodes.

Acknowledgment. This work was supported by National Research Foundation of Korea Grant funded by the Korean Government (Grants 2010-0001637, M10703001067-08M0300-06711-Nano2007-02943, KRF-2008-313-C00390, and 2009-0072467).

References and Notes

(1) Fleischmann, M.; Hendra, P. J.; McQuillan, A. J. *Chem. Phys. Lett.* **1974**, *26*, 163.
(2) Jeanmaire, D. L.; Van Duyne, R. P. *J. Electroanal. Chem.* **1977**, *84*, 1.
(3) Moskovits, M. *Rev. Mod. Phys.* **1985**, *7*, 209.
(4) Otto, A.; Mrozek, I.; Grabhorn, H.; Akemann, W. *J. Phys.: Condens. Matter.* **1992**, *4*, 1143.
(5) Campion, A.; Kambhampati, P. *Chem. Soc. Rev.* **1998**, *27*, 241.
(6) Nie, S.; Emory, S. R. *Science* **1997**, *275*, 1102.
(7) Kneipp, K.; Kneipp, H.; Itzkan, I.; Dasari, R.; Feld, M. *Chem. Rev.* **1999**, *99*, 2957.
(8) Krug, J. T.; Wang, G. D.; Emory, S. R.; Nie, S. *J. Am. Chem. Soc.* **1999**, *121*, 9208.
(9) Emory, S. R.; Haskins, S.; Nie, S. *J. Am. Chem. Soc.* **1998**, *120*, 8009.
(10) Xu, H.; Bjerneld, E. J.; Käll, M.; Borjesson, L. *Phys. Rev. Lett.* **1999**, *83*, 4357.
(11) Michaels, A. M.; Jiang, J.; Brus, L. *J. Phys. Chem. B* **2000**, *104*, 11965.
(12) Moskovits, M. *J. Raman Spectrosc.* **2005**, *36*, 485.
(13) Lee, S. J.; Morrill, A. R.; Moskovits, M. *J. Am. Chem. Soc.* **2006**, *128*, 2200.
(14) Lee, S. J.; Guan, Z.; Xu, H.; Moskovits, M. *J. Phys. Chem. C* **2007**, *111*, 17985.
(15) Deng, X.; Braun, G. B.; Liu, S.; Sciortino, P. F.; Koefer, Bob., Jr.; Tombler, T.; Moskovits, M. *Nano Lett.* **2010**, *10*, 1780.
(16) Lee, S. J.; Baik, J. M.; Moskovits, M. *Nano Lett.* **2008**, *8*, 3244.
(17) Tian, Z. Q.; Ren, B.; Mao, B. W. *J. Phys. Chem. B* **1997**, *101*, 1338.
(18) Tian, Z. Q.; Gao, J. S.; Li, X. Q.; Yao, L.; Ren, B.; Huang, Q. J.; Cai, W. B.; Liu, F. M.; Mao, B. W. *J. Raman Spectrosc.* **1998**, *29*, 703.
(19) Tian, Z. Q.; Ren, B.; Wu, D.-Y. *J. Phys. Chem. B* **2002**, *106*, 9463.
(20) Tian, Z. Q.; Ren, B.; Li, J.-F.; Yang, Z.-L. *Chem. Commun.* **2007**, 3514.
(21) Tian, N.; Zhou, Z.-Y.; Sun, S.-G.; Cui, L.; Ren, B.; Tian, Z. Q. *Chem. Commun.* **2006**, 4090.
(22) Cai, W. B.; Ren, B.; Li, X. Q.; She, C. X.; Liu, F. M.; Cai, X. W.; Tian, Z. Q. *Surf. Sci.* **1998**, *406*, 9.
(23) Futamata, M.; Keim, E.; Bruckbauer, A.; Schumacher, D.; Otto, A. *Appl. Surf. Sci.* **1996**, *100*, 60.
(24) Futamata, M. *Appl. Opt.* **1997**, *36*, 364.
(25) Creighton, J. A.; Eadon, D. G. *J. Chem. Soc., Faraday Trans* **1991**, *87*, 3881.
(26) Henglein, A.; Ershov, B. G.; Malow, M. *J. Phys. Chem.* **1995**, *99*, 14129.
(27) Janata, E.; Henglein, A.; Ershov, B. *J. Phys. Chem.* **1996**, *100*, 1989.
(28) Kim, N. H.; Kim, K. *Chem. Phys. Lett.* **2004**, *393*, 478.
(29) Kim, N. H.; Kim, K. *J. Raman Spectrosc.* **2005**, *36*, 623.
(30) Kim, N. H.; Kim, K. *J. Phys. Chem. B* **2006**, *110*, 1837.
(31) Bigall, N. C.; Härtling, T.; Klose, M.; Simon, P.; Eng, L. M.; Eychmüller, A. *Nano Lett.* **2008**, *8*, 4588.
(32) Grabar, K. C.; Freeman, R. G.; Hommer, M. B.; Natan, M. *J. Anal. Chem.* **1995**, *67*, 735.
(33) Bard, A. Faulkner, L. R. *Electrochemical Methods: Fundamentals and Applications*, 2nd ed., Wiley: New York, 2001.
(34) Park, S.; Yang, P.; Corredor, P.; Weaver, M. J. *J. Am. Chem. Soc.* **2002**, *124*, 2428.

(35) Morzek, M. F.; Xie, Y.; Weaver, M. *J. Anal. Chem.* **2001**, *73*, 5953.
(36) Zou, S.; Weaver, M. *J. Anal. Chem.* **1998**, *70*, 2387.
(37) Gómez, R.; Pérez, J. M.; Solla-Gullón, J.; Montiel, V.; Aldez, A. *J. Phys. Chem. B* **2004**, *108*, 9943.
(38) Gómez, R.; Solla-Gullón, J.; Pérez, J. M.; Aldez, A. *J. Raman Spectrosc.* **2005**, *36*, 613.
(39) Joo, T. H.; Kim, M. S.; Kim, K. *J. Raman Spectrosc.* **1987**, *18*, 57.
(40) Bryant, M. A.; Joa, S. L.; Pemberton, J. E. *Langmuir* **1992**, *8*, 753.
(41) Maxwell, D. J.; Emory, S. R.; Nie, S. *Chem. Mater.* **2001**, *13*, 1082.
(42) Yu, H. Z.; Zhang, J.; Zhang, H. L.; Liu, Z. F. *Langmuir* **1999**, *15*, 16.
(43) Wan, L. J.; Terashima, M.; Noda, H.; Osawa, M. *J. Phys. Chem. B* **2000**, *104*, 3563.
(44) Borchert, H.; Shevchenko, E. V.; Robert, A.; Mekis, I.; Kornowski, A.; Grübel, G.; Weller, H. *Langmuir* **2005**, *21*, 1931.
(45) Xuan, S.; Wang, Y. J.; Yu, J. C.; Leung, K. C. *Chem. Mater.* **2009**, *21*, 5079.
(46) Osawa, M.; Matsuda, N.; Yoshii, K.; Uchida., I. *J. Phys. Chem.* **1994**, *98*, 12702.
(47) Huang, Y.-F.; Zhu, H.-P.; Liu, G.-K.; Wu, D.-Y.; Ren, B.; Tian, Z. Q. *J. Am. Chem. Soc.* **2010**, *132*, 9244.
(48) Kim, K.; Yoon, J. K. *J. Phys. Chem. B* **2005**, *109*, 20731.
(49) Yoon, J. K.; Kim, K.; Shin, K. S. *J. Phys. Chem. C* **2009**, *113*, 1769.
(50) Kim, K.; Lee, H. B.; Yoon, J. K.; Shin, D.; Shin, K. S. *J. Phys. Chem. C* **2010**, *114*, 13589.
(51) Han, S. W.; Lee, I.; Kim., K. *Langmuir* **2002**, *18*, 182.
(52) Lee, S. J.; Kim, K. *Chem. Phys. Lett.* **2003**, *378*, 122.
(53) Kim, K.; Lee, I.; Lee, S. J. *Chem. Phys. Lett.* **2003**, *377*, 201.
(54) Kim, K.; Lee, I. *Langmuir* **2004**, *20*, 7351.
(55) Kim, K.; Lee, S. J.; Kim, K. L. *J. Phys. Chem. B* **2004**, *108*, 16208.
(56) Lombardi, J. R.; Birke, R. L. *J. Phys. Chem. C* **2008**, *112*, 5605.

JP1078532